

PAPER • OPEN ACCESS

## Fabrication routes for advanced first wall design alternatives

To cite this article: M. Rieth *et al* 2021 *Nucl. Fusion* **61** 116067

View the [article online](#) for updates and enhancements.

### You may also like

- [Development of 410S-Y<sub>2</sub>O<sub>3</sub> oxide dispersion strengthened steel prepared by a powder metallurgy technique](#)  
T Sudiro, R C Ekaputra, K A Z Thosin et al.
- [Research progress on preparation technology of oxide dispersion strengthened steel for nuclear energy](#)  
Jianqiang Wang, Sheng Liu, Bin Xu et al.
- [Investigation of high-temperature oxidation behavior of silicon added 14Cr nanostructured ferritic alloys synthesized via mechanical alloying and spark plasma sintering](#)  
Wahida R Ilaham, Ram S Maurya and Tapas Laha







**IOP | ebooks™**

Bringing together innovative digital publishing with leading authors from the global scientific community.

Start exploring the collection—download the first chapter of every title for free.

# Fabrication routes for advanced first wall design alternatives

M. Rieth<sup>1,\*</sup> , M. Dürrschnabel<sup>1</sup>, S. Bonk<sup>1</sup>, S. Antusch<sup>1</sup>, G. Pintsuk<sup>2</sup> , G. Aiello<sup>3</sup>, J. Henry<sup>4</sup>, Y. de Carlan<sup>4</sup>, B.-E. Ghidersa<sup>5</sup> , H. Neuburger<sup>5</sup>, J. Rey<sup>5</sup>, C. Zeile<sup>5</sup>, N. De Wispelaere<sup>6</sup>, E. Simondon<sup>1</sup>  and J. Hoffmann<sup>1</sup>

<sup>1</sup> Karlsruhe Institute of Technology, Institute for Applied Materials, 76344 Eggenstein-Leopoldshafen, Germany

<sup>2</sup> Forschungszentrum Jülich GmbH, Institut für Energie- und Klimaforschung – Plasmaphysik, 52425 Jülich, Germany

<sup>3</sup> EUROfusion, PPPT, 85748 Garching, Germany

<sup>4</sup> Université Paris-Saclay, CEA, Service de Recherches Métallurgiques Appliquées, 91191, Gif-sur-Yvette, France

<sup>5</sup> Karlsruhe Institute of Technology, Institute for Neutron Physics and Reactor Technology, 76344 Eggenstein-Leopoldshafen, Germany

<sup>6</sup> OCAS NV, Pres. J.F. Kennedylaan 3, 9060 Zelzate, Belgium

E-mail: [michael.rieth@kit.edu](mailto:michael.rieth@kit.edu)

Received 8 June 2021, revised 11 August 2021

Accepted for publication 9 September 2021


Published 14 October 2021



## Abstract

In future nuclear fusion reactors, plasma facing components have to sustain specific neutron damage. While the majority of irradiation data provides a relatively clear picture of the displacement damage, the effect of helium transmutation is not yet explored in detail. Nevertheless, available results from simulation experiments indicate that 9%-chromium steels will reach their operating limit as soon as the growing helium bubbles extent a critical size. At that point, the material would most probably fail due to grain boundary embrittlement. In this contribution, we present a strategy for the mitigation of the before-mentioned problem using the following facts. (1) The neutron dose and related transmutation rate decreases quickly inside the first wall of the breeding blankets, that is, only a plasma-near area is extremely loaded. (2) Nanostructured oxide dispersion strengthened (ODS) steels may have an enormous trapping effect on helium, which would suppress the formation of large helium bubbles for a much longer period. (3) Compared to conventional steels, ODS steels also provide improved irradiation tensile ductility and creep strength. Therefore, a design, based on the fabrication of the plasma facing and highly neutron and heat loaded parts of blankets by an ODS steel, while using EUROFER97 for everything else, would extend the operating time and enable a higher heat flux. Consequently, we (i) developed and produced 14%Cr ferritic ODS steel plates and (ii) optimized and demonstrated a scalable industrial production route. (iii) We fabricated a mock-up with five cooling channels and a plated first wall of ODS steel, using the same production processes as for a real component. (iv) Finally, we performed high heat flux tests in the Helium Loop Karlsruhe, applying a few hundred short and a few 2 h long pulses, in which the operating temperature limit for EUROFER97 (i.e. 550 °C) was finally exceeded by 100 K. (v) Thereafter, microstructure and defect analyses did not reveal critical defects or recognizable damage. Only a heat affected zone in the EUROFER/ODS steel interface could

\* Author to whom any correspondence should be addressed.

 Original content from this work may be used under the terms of the [Creative Commons Attribution 4.0 licence](https://creativecommons.org/licenses/by/4.0/). Any further distribution of this work must maintain attribution to the author(s) and the title of the work, journal citation and DOI.

be detected. However, a solution to prohibit the formation of such heat affected zones is given. These research contributions demonstrate that the use of ODS steel is not only feasible and affordable but could make a decisive difference in the future design and performance of breeding blankets.

Keywords: blanket first wall, oxide dispersion strengthened (ODS) steel, high heat flux test, helium cooling loop, materials technology, dissimilar joints, diffusion bonding

(Some figures may appear in colour only in the online journal)

## 1. Introduction

In the present pre-conceptual design phase, the operating limit of the starter blanket for a European demonstration fusion reactor (DEMO) is predefined by a neutron dose of 20 dpa. In a second stage, a more advanced blanket will be tested with an extended lifetime corresponding to about 50 dpa. Based on today's material technology, this can only be achieved by increasing the operating temperature in the steel structures to 350 °C and above. Therefore, the coolant for the second (advanced) blanket of the European DEMO reactor should/will be helium gas [1–4].

Regardless of the different breeding blanket concepts, the plasma-facing surface, and a layer of several millimetres is the highest loaded part with regard to thermal as well as neutron load. Therefore, at least three main damage modes have to be taken into account: (1) thermal fatigue due to the pulsed plasma operation with some ten-thousand cycles, (2) neutron irradiation hardening and embrittlement as a consequence of displacement damage, and (3) material damage due to transmutation products, i.e. in steels this mainly leads to the formation of helium bubbles (but also hydrogen is produced). While most irradiation data give a relatively clear view on the displacement damage, which is mainly responsible for the observed irradiation hardening, the effect of gas transmutation—i.e. especially helium production in ferritic/martensitic 9Cr-steels—has not been explored yet sufficiently. Nevertheless, available results indicate that EUROFER-type steels (the selected base and reference material within the European fusion project) will reach their operating limit when the formation of helium bubbles reaches a critical amount or size, which then leads to brittle fracturing [5–7].

For future power fusion power plants, operating temperatures in the range of 450–550 °C (or maybe even higher) would be an effective measure to reduce irradiation hardening significantly (see, for example, [8–13]). In this case, the lifetime of helium-cooled breeding blankets would then be determined mainly by the thermo-mechanical load response (thermal fatigue) and by the accumulation and growth of helium bubbles.

In this paper, we present a possible strategy for the mitigation of the before-mentioned design limiting issues by making use of the following facts and assumptions: (1) neutron dose and related transmutation rates decrease significantly from the first wall towards the back plates, that is, only a plasma-near

volume of the blanket is critically high loaded [14, 15]. (2) Nanostructured oxide dispersion strengthened (ODS) steels can have an enormous trapping effect on helium, which then slows down the formation of critically big helium bubbles [16]. (3) Compared to conventional steels, ODS steels show better fatigue (and creep) resistance. That is, they can be operated at higher temperatures, which would substantially reduce irradiation hardening [17–19].

In summary, producing the plasma facing, highly neutron and heat loaded parts in blankets by an ODS steel (while using EUROFER steel for everything else), would allow a higher heat flux, a longer and safer operating period, and possibly more degrees of freedom in the design. A first step in this direction, which is not so ambitious but might still be interesting, can yield valuable information: if we focus just on the superior thermo-mechanical properties, an ODS steel layer on top of the blanket first wall could in principle allow higher coolant temperatures and longer component operating-times. For this, an ODS steel plating of 2–3 mm on top of a EUROFER based cooling structure (breeding blanket with cooling channels according to the current designs) would be required.

A first verification of the before-mentioned strategy took about 7 years—starting with the idea and ending after the final destructive post-testing analyses—during which we followed (most often in parallel) four main lines of research, development, and investigation: (1) production of thin ODS steel plates, also on a larger scale, i.e. in the order of 100 kg; (2) development and selection of robust fabrication processes; (3) design and manufacture of a testable DEMO breeding blanket first wall mock-up; and (4) cyclic high heat flux loading in a helium cooling loop.

The mock-up we discuss and report in this paper is a first-of-its-kind, worldwide. For both, ODS plate and mock-up fabrication, we placed the emphasis on available or technologically scalable processes that are especially appropriate for industrial applications. Another novelty is the cyclic high heat flux test in a helium cooling loop, in which the surface temperature of a first wall mock-up could be intentionally increased above the common 550 °C operating limit of the nuclear fusion steel EUROFER97.

## 2. Materials

The manufacturing processes and the most important properties of a broad range of low-activating ODS

**Table 1.** Rolling scheme. Reduction and plate thickness (including capsule material at the surfaces) after each rolling pass.

Pass No.	Initial	1	2	3	4	5	6	7	8	9	10	11
Reduction (%)	—	16	20	22	20	20	15	20	20	20	20	20
Thickness (mm)	65	54.6	43.7	34.1	27.3	21.8	18.5	14.8	11.9	9.5	7.6	6.1

steels are well-known and have been widely explored, studied, and discussed (an overview is given in [20–23] and references therein). Out of this knowledgebase, a ferritic ODS steel with the specification (13–14)Cr–(1–1.2)W–(0.2–0.3)Ti–(0.2–0.3)Y<sub>2</sub>O<sub>3</sub> (numbers in weight %) was chosen as the plating material for this project. The reason for the lower as usual Ti and Y<sub>2</sub>O<sub>3</sub> concentrations is to reduce the recrystallization temperature. A higher density of Ti–Y-oxide particles could cause problems during plate manufacturing (e.g. abnormal grain-growth during recrystallization). However, with these specifications the final product was expected to still have very good high-temperature properties, which would meet the requirements for the chosen application, although the creep performance would be somewhat lower than that of a 14Cr alloy with higher Ti and Y concentrations.

The materials production was separated in two parts. (1) A short-term production of a lab-scale batch was used for the mock-up fabrication. (2) A separate medium-scale plate fabrication study was performed over several years to demonstrate the feasibility of commercial production routes of large ODS steel batches for structural applications.

### 2.1. ODS steel—lab scale production

First, we produced a lab-scale batch of ODS steel that was tailored to the mock-up fabrication. For that, pre-alloyed powder (5 kg) was mechanically alloyed together with yttria powder in hydrogen atmosphere in an industrial attritor ball mill at Zoz GmbH, Germany. The as-milled powder with a chemical composition of Fe–13Cr–1.1W–0.3Ti–0.3Y<sub>2</sub>O<sub>3</sub> was packed in argon and sent to KIT for further processing in an argon-filled glove-box to protect the powder from oxidation in air. Here, the fraction between 45 μm and 90 μm powder particle diameter was taken out by sieving. From this, 2.6 kg were filled in a cylindrical 316L stainless steel capsule (diameter: 80 mm, height: 170 mm). After degassing at 400 °C, the capsule was sealed and then hot-isostatic pressed at 1100 °C with a pressure of 100 MPa for 2 h holding time in a KIT facility. After taking off the top and bottom of the capsule, it was sent to OCAS, Belgium for tempering and hot-cross-rolling at 1050 °C. The rolling scheme with the reduction for each step is given in table 1. After pass number 5, the capsule was reheated for 10 min. When the rolling temperature of 1050 °C was reached again, the capsule was turned for 90° and rolled in this direction.

The wall of the stainless-steel capsule was left on during the whole rolling process. This reduced the thermal shock to the material, and therefore, prevented hot cracking and also oxidation.

An electron back-scatter diffraction (EBSD) scan of the plate in the transvers view is shown in figure 1. The map is

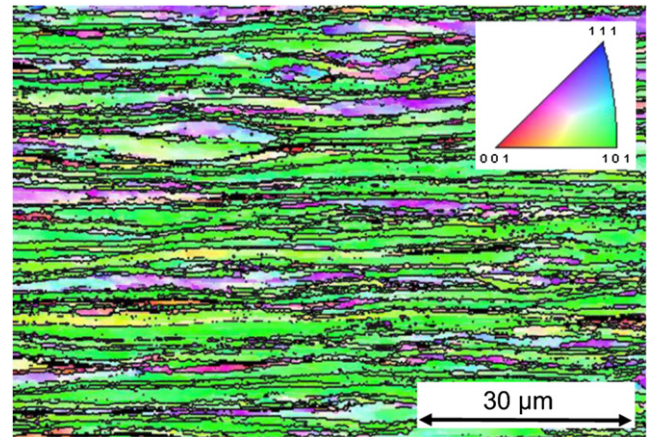


**Figure 1.** Microstructure of the ODS steel plate after rolling. EBSD scan in transverse view along rolling direction with a step size 300 nm.

calculated along the rolling direction (RD) and displays a strong  $\langle 101 \rangle$  orientation (green colour) of the grains, which also have a high aspect ratio with a distinct elongation along the RD. The grain size is in a typical range for ferritic ODS alloys. Looking more into detail reveals a pronounced substructure within the larger grains, in which sometimes high orientation gradients occur. This has also been reported for other ferritic ODS alloys produced in a similar way.

### 2.2. Intermediate-scale plate fabrication

One of the main objectives of this project was the manufacturing of 2–3 mm thick plates in a quantity of about 100 kg as a demonstration for a feasible commercial production route. For this, several companies were involved at the different stages of the industrial processes. Nanoval was the powder-producer, Plansee was responsible for mechanical alloying, Aubert–Duval was designated for powder vacuum canning, Bodycote was selected for hot isostatic pressing, and OCAS oversaw the hot-cross rolling optimization of the plates and the final cold rolling. Coordination, quality assurance, and characterization was performed by CEA.

Nanoval produced a total of 164 kg of powder by atomization with argon gas. The powder particles showed a mean diameter ( $d_{50}$ ) of about 30 μm with a constraint on 90% of the procurement of particle dimensions lower than 120 μm. After production, the powder was shipped in containers—each of 10–14 kg—under protective argon atmosphere to CEA Saclay. The particle size distribution, measured by a laser diffraction sensor (HELOS instrument), was in good agreement with the specifications. A chemical analysis revealed that the titanium content of 0.16 wt.% was slightly too low (compared to the specification of 0.2 wt.%), but the batch was accepted anyway.



**Table 2.** Chemical analysis (in weight % and weight ppm) of the mechanically alloyed (milled) powder (according to Plansee).

	Cr	C	Mn	W	N	O	Y	Ti	Ni	H
Milled powder	13.5%	164 ppm	917 ppm	0.99%	78 ppm	0.117%	0.146%	0.16 %	559 ppm	57 ppm

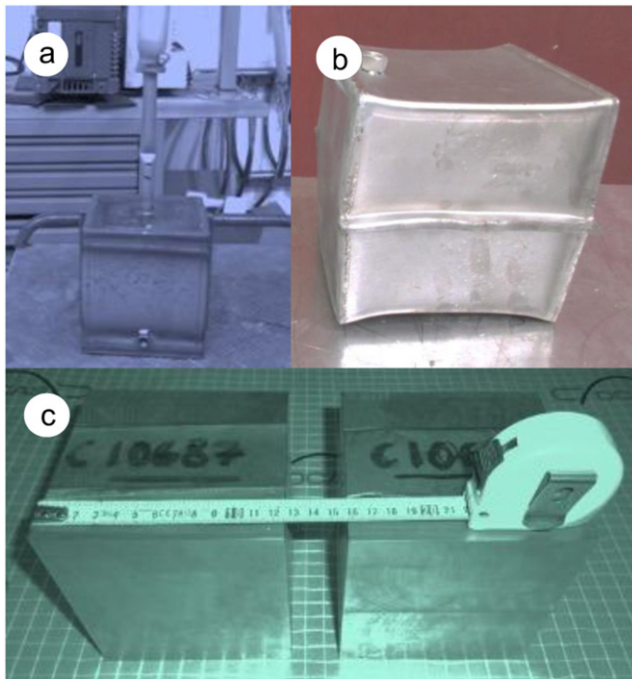


**Figure 2.** (a) Evacuation of a HIP container. (b) Container after hot-isostatic pressing. (c) Semi-finished product: consolidated powder blocks of 125 mm × 125 mm × 125 mm.

So, 140 kg of the powder was sent to Plansee for mechanical alloying (MA). Plansee added 0.2 ± 0.05 wt.%  $Y_2O_3$  powder and performed MA in an industrial facility under pure hydrogen. Then the milled powder was sieved, which left 109 kg of powder with a particle size lower than 100  $\mu m$ . This corresponds to an output of about 75% of the total amount of material. The final chemical composition is compiled in table 2. Finally, the milled and sieved powder was filled in plastic containers under air and sent back to CEA.

The next step—powder consolidation—was conducted by the companies Aubert et Duval and Bodycote. For that, two containers of 316 steel were fabricated, filled with the powder, degassed, and sealed (Aubert et Duval). Then, the containers were hot iso-statically pressed by Bodycote at 1160 °C for 3 h at 102 MPa. Compared to the lab-scale production, the consolidation temperature and period were increased due to the increased volume and different geometry of the capsules. Finally, two blocks were machined to the size 125 mm × 125 mm × 125 mm (each of 15 kg), as illustrated in figure 2.

With these semi-finished products, rolling studies were then performed at OCAS. The initial process parameters were similar to those of the lab-scale fabricated plate. But we applied slight modifications (e.g. increase of the initial rolling temperature without reheating during the rolling process, or the final cold rolling steps) to facilitate industrial procedures. To

avoid decarburization, the first block was packed in a stainless-steel strip before being rolled from 125 mm to 63 mm with a reduction of 10% per pass. The initial rolling temperature was 1100 °C. In the subsequent hot-rolling passes, the temperatures were not acquired. However, a conservative estimate leads to a temperature drop less than about 100–200 K. Due to the low thickness to length ratio, the ends of the ODS sheet take a V shape in rolling direction, which often promotes the initiation of cracks. Therefore, after reaching a thickness of 63 mm, we continued with cross-rolling. For this, the plate was heated to 1100 °C again to recover ductility.

During cross rolling, a formation of small cracks on the edges of the sheets could be observed. Fortunately, the length of these small cracks remained stable, and therefore, the ODS steel could be further hot-rolled to a thickness of 5 mm.

Cold rolling hard materials such as ODS steels is a sensitive and non-trivial process. Therefore, different studies were conducted on instrumented rolling mills, which display and record displacements and forces during processing the plates. After 15 rolling steps, reaching a thickness of about 2.6 mm, the sheet did no longer deform and the mismatch between cylinder gap and sheet thickness was reaching about 0.3 mm. Hence, a heat treatment (1100 °C for 5 min) was performed to reduce the hardness and to prevent cracking. In a separate study, where hardness was measured after different iso-chronal annealing experiments, we validated that this recovery treatment did not lead to recrystallization. Finally, cold-rolling was continued to a plate thickness of 2 mm.

With this manufacturing route, two sheets of 1200 mm × 230 mm × 2 mm were produced. For the second block, in principle the same plate production route was set up. But to avoid the V-shape deformation at the rolling ends during hot-rolling as well as for a reduction of cracks at the edges of the sheet, the ODS steel block was embedded in a bigger cylindrical steel block. After hot-rolling, the surrounding steel was removed and cross-rolling was performed on the ODS steel block alone. By this technique, 4 additional plates of 3 mm (1000 mm × 100 mm) and 2 mm (1300 mm × 100 mm) thickness could be produced (see figure 3).

### 3. Design

The objective of the mock-up design was to get a down-sized representative model of a typical first wall, e.g. that of a DEMO reactor, which may be installed in the Helium Loop Karlsruhe (HeLoKa) for high heat flux tests. There are four DEMO blanket concepts: two with water and two using helium as a coolant. In principle, the ODS plated first wall configuration could yield advantages for all concepts, e.g. in terms of longer life-times. But the water temperature is limited to a sub-critical operation regime (super-critical water cooling has not



**Figure 3.** ODS steel plates after rolling. From the second block, two 2 mm and two 3 mm thick plates were produced by hot and cold-rolling.

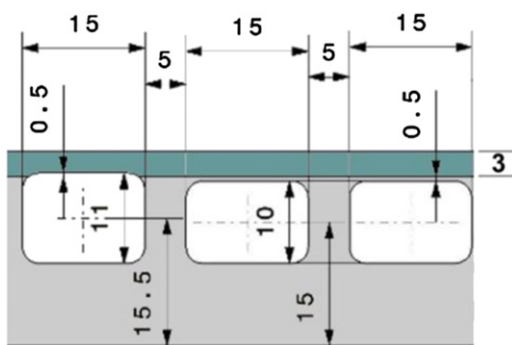


**Figure 4.** Geometry of the cooling channels. The cooling channel dimensions are 10 mm (height) by 15 mm (width) with a 2 mm radius at the corners. The channel in the middle (the left one in the drawing) is higher by 1 mm compared to the other four. That is, this channel cross-section exceeds the baseplate of EUROFER97/2 (light grey) and is machined into the ODS steel plating (dark grey). That is, the diffusion bond-lines run along both upper corners. This means that we have placed the potentially weakest points (the weld seam) in the area of highest stress (this is due to stress concentration along the 2 mm radii of the corners).

been taken seriously into account for a DEMO reactor). Therefore, the benefit of ODS steel plating might be higher for the helium cooled concepts due to the possibility to increase the operating temperature. From a fabrication point of view (with a focus on the ODS steel plating), there are no big differences between the blanket concepts, either. Thus, we decided to use the helium cooled pebble bed (HCPB) breeding blanket concept as a reference for the mock-up design. Detailed outlines of the design is given, for example, in [24–26] and references therein.

We provided our mock-up with five cooling channels. The geometry and details of the ODS steel plating are depicted in figure 4. The channel inner surfaces were machined flat and they were not equipped with swirls or other turbulence enhancers. Note: one channel was intentionally misaligned, so that the weld seam of the ODS steel plating appeared at the corner, which is the highest stressed location. This generated two lines of preferential crack initiation (see also section 5.1).

## 4. Fabrication processes

As already mentioned in the introduction, we placed an emphasis on available or technologically scalable processes that are especially appropriate for industrial applications. Therefore, prior to the mock-up fabrication, we analysed common fabrication routes for their applicability in an industrial environment. The following three subsections review briefly the topics (1) surface machining, (2) diffusion bonding, and (3) machining of long cooling channels.

### 4.1. Surface machining

For an efficient first wall fabrication, the application of different milling processes is probably unavoidable. This applies particularly to the joining of parts by diffusion bonding, but also to all cases, for which a specific surface quality (roughness) is important. The following analyses are based on studies that were partly accomplished within the former European fusion development agreement.

**4.1.1. Milling.** For this survey, several surfaces have been fabricated on pieces of EUROFER97/2 (heat 993 402, treatment: 980 °C/0.5 h, air quenching, 760 °C/2 h) by dry milling. Five standard milling procedures (ID: 1–5) have been applied (details are given in table 3 and figure 5), which led to different surfaces structures (see figure 6). For comparison, a reference surface (ID: Ref) was prepared by metallographic polishing, i.e. without recognizable roughness.

The images in figure 6 show clearly that the surfaces ID 1 and 2, which were fabricated by the 4 teeth radius cutter (figure 5(a)), are rougher compared to ID 3–5. Both reveal distinct distortions due to chipping. The surfaces look like some chunks had been broken off from the surface. Surprisingly, roughness profiles (derived from 3d SEM image processing, normal to the milling direction) of all surfaces look quite similar and there are no noticeable differences in the characteristics.

**4.1.2. Hardness effect.** As has been shown, irregular shaped surface distortions appeared in connection with the four-teeth radius cutter. They are due to specific chip removal conditions. Chipping strongly depends on the general material properties (ductility, hardness, etc), that is, ductile or soft materials tend to ‘smear’ during milling while chip removal from hard surfaces is typically superior.

Since hard materials cause higher wear, there is an optimum for both surface quality and abrasion of the tools, which in turn is relevant for cost efficiency. In the case of the martensitic EUROFER97/2 steel, it is easy to adjust hardness by appropriate heat treatments. This has been investigated by performing two different heat treatments prior to surface fabrication. One sample has been fabricated after an austenitization treatment of 980 °C/0.5 h and subsequent quenching in air (ID: 2b). Another one was fabricated after austenitization followed by tempering at the lowest possible and still effective temperature, i.e. at 630 °C for 2 h (ID: 2c). The first one led to slightly harder surfaces.

**Table 3.** Milling and cutter parameters for the surface treatment performed by an industrial CNC milling machine. VC: cut velocity ( $\text{mm s}^{-1}$ ), fz: feed rate per tooth ( $\text{mm s}^{-1}$ ), S: rotations (1/s), ap: infeed (mm), F: feed rate ( $\text{mm s}^{-1}$ ).

ID	VC	fz	S	ap	F	Tool
Ref (7)						Polishing wheel
1 (8)	50	0.05	995	0.05	190	Hard metal radius, $\text{Ø}16$ mm, 4 teeth, rolling
2 12	50	0.08	995	0.15	318	Hard metal radius, $\text{Ø}16$ mm, 4 teeth, pitch $20^\circ$
3 (10)	100	0.08	510	0.15	245	Knife head, $\text{Ø}63$ mm, $6 \times 90^\circ$ 08M-MM plates
4	100	0.07	510	0.15	178	Knife head, $\text{Ø}63$ mm, $5 \times 45^\circ$ E-M plates
5	80	0.1	405	0.15	202	Knife head, $\text{Ø}63$ mm, $5 \times 45^\circ$ K-MM plates

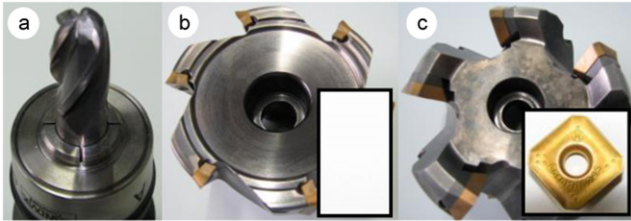


**Figure 5.** (a) 4 teeth radius cutter used for preparing sample ID 1 and 2. (b) 6 teeth knife head in combination with Sandvik cutter plates 2030 R390-11 T3 08M-MM (lower right insert) used for sample ID 3. (c) 5 teeth knife head with Sandvik cutter plates 2040 R245-12 T3 K-MM and 1025 R245-12 T3 E-M (lower right insert) used for sample ID 5 and 4.

After the heat treatments, the surfaces were milled by the fabrication parameters for ID 2. The results can be seen in figure 7. Compared to sample ID 2 (which were fabricated after standard heat treatment, i.e. after tempering at  $760^\circ\text{C}$ ), the harder microstructure of specimens ID 2b and 2c resulted in much smoother surfaces. With this finding, the restriction to specific milling tools seems to be obsolete.

#### 4.2. Diffusion bonding

Weld samples with pairs of EUROFER97/2 pieces were fabricated by hot isostatic pressing (HIP). The weld surfaces with cross sections of  $25\text{ mm} \times 25\text{ mm}$  were machined as described in the previous section (ID 1–5 and a polished reference surface). Then the samples were tight sealed by a 0.5 mm deep circumferential electron beam weld line around the joints. Thereafter, diffusion bonding was performed by a HIP cycle at  $25\text{ MPa}/1050^\circ\text{C}/2\text{ h}$ , followed by a standard heat treatment at  $980^\circ\text{C}/0.5\text{ h}$ , air quenching, and  $760^\circ\text{C}/2\text{ h}$ .

Charpy specimens (KLST type,  $3\text{ mm} \times 4\text{ mm} \times 27\text{ mm}$ , 1 mm notch depth) were fabricated perpendicular to the weld line, joint surface, and rolling direction, while the notches were oriented parallel to the weld surface (see figure 8). Specimen size and testing conditions (support span 22 mm, 50 J pendulum) followed European standards. The test results are presented in figure 9.

Surfaces ID 1 and 2 have been produced using the same milling cutter but with different parameters. Both surfaces (white and grey circles) showed about the same density of cavities. Compared to the unwelded EUROFER97/2 base material (white diamonds) and the reference sample (diffusion bonded sample with polished surfaces, black diamonds), the Charpy

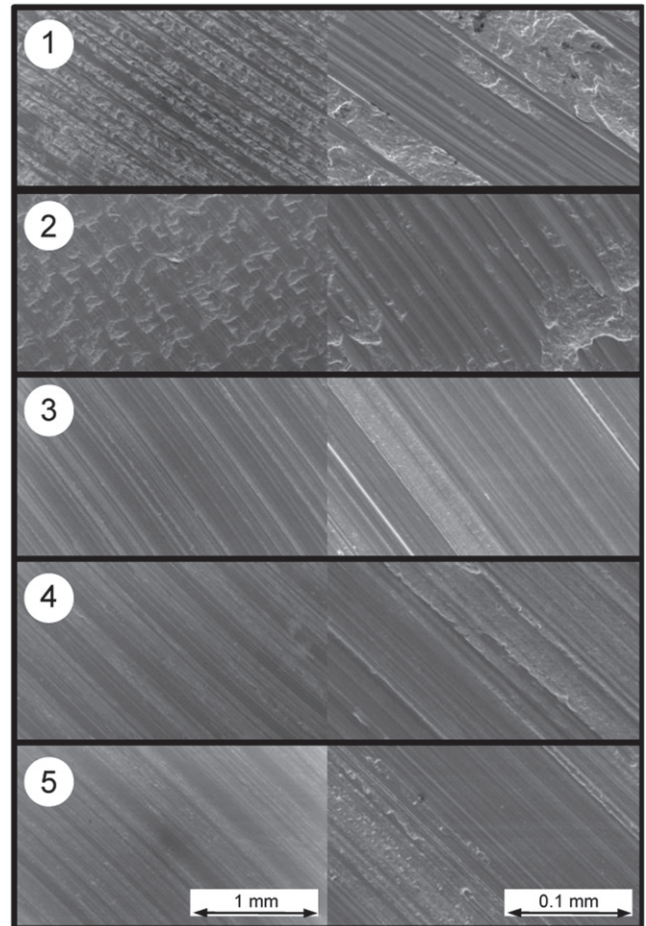


**Figure 6.** Scanning electron microscopy images of the surfaces ID 1–5 produced according to the parameters given in table 3.

properties are significantly deteriorated, while ID 4 and 5 (different cutting plates in a five-knife head tool) show about the same toughness as the base and reference material.

These differences can be directly linked to the surface structures (see figure 6), and therefore, to the different chipping behaviour. However, the Charpy results of specimens from sample ID 3 do not fit into the picture since the toughness values are clearly lower than those of the reference material (but not as bad as ID 1 and 2), even though the surface structure is very similar to ID 4 and 5.



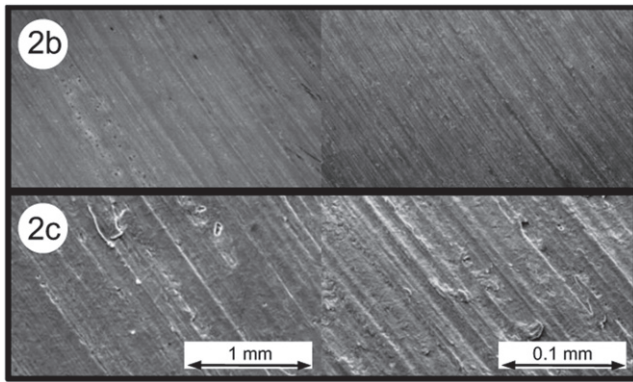


**Figure 7.** Scanning electron microscopy images of surfaces that have been produced by the parameters for ID 2 (see table 3) with a preceding heat treatment of 980 °C/0.5 h and subsequent air quenching (2b), and 980 °C/0.5 h, air quenching, and 630 °C/2 h (2c).

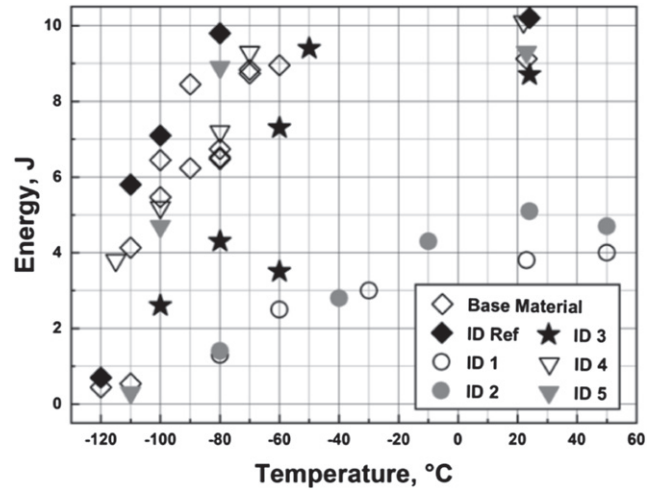


**Figure 9.** Charpy test results of samples with different surface machining after diffusion bonding by one HIP cycle at 25 MPa/1050 °C/2 h, followed by a standard heat treatment at 980 °C/0.5 h, air quenching, and 760 °C/2 h.

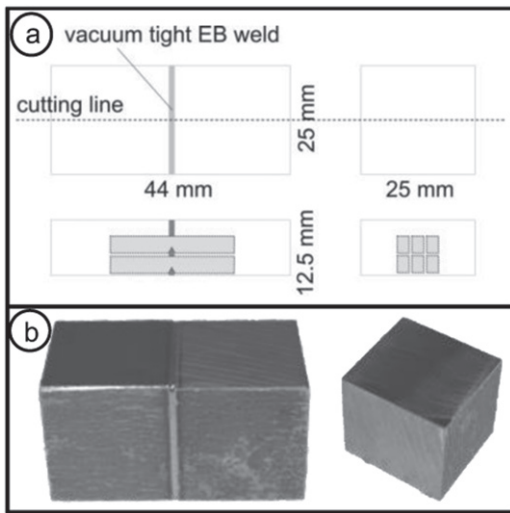


**Figure 8.** (a) Fabrication scheme of the weld samples and orientation of the Charpy specimens. (b) Photo of a weld sample before and after sealing by an electron beam weld prior to HIP.

With this result it rather questionable to use surface structures or roughness as a measure for the diffusion bond performance.

**4.2.1. HIP parameters.** The reason behind the relatively low pressure of only 25 MPa in the previous diffusion bond study was the possible application for fabricating the cooling channels of a first wall or blanket caps. For plating the first wall, we don't have these restrictions. Therefore, we examined the effect of a higher HIP pressure by performing a second cycle on sample ID 2.

The result of such a HIP cycle at 1050 °C with 100 MPa for 2 h is illustrated in figure 10. It is remarkable that even in the reference sample, which performed slightly better in the Charpy tests as the EUROFER97/2 base material (see figure 9), the weld surface is still recognizable. The same is true for sample ID 5, which Charpy properties are comparable to those of the base material. The cross-section of sample 2

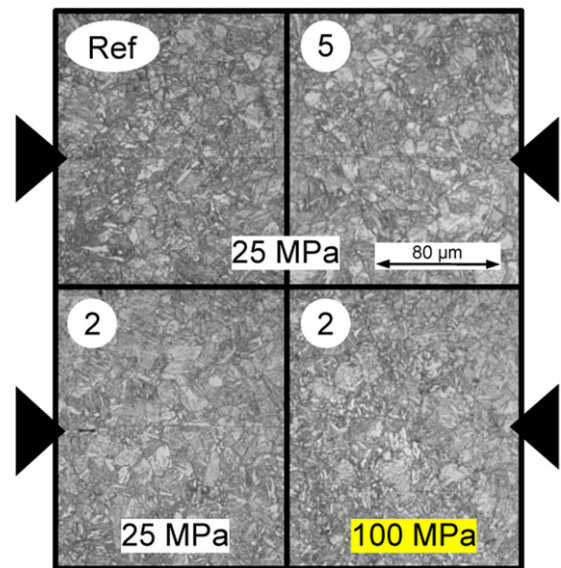


**Figure 10.** SEM images of cross-sections from samples with different surface machining after diffusion bonding by one HIP cycle at 25 MPa/1050 °C/2 h (IDs: Ref, 5, and 2). In these three cases, the weld surface (indicated by the black arrows) is still recognizable. The lower right SEM image shows the same cross-section of sample ID 2 after a second HIP cycle at 100 MPa/1050 °C/2 h. The weld surface cannot be identified anymore.

reveals the reason for its low toughness: remaining cavities in the weld surface.

These cavities (and also the recognizable weld surface) are fully removed by the HIP cycle at 100 MPa pressure, and this in turn, has improved the Charpy properties, which are now as good as those of the base material.

**4.2.2. Corrosion and contamination.** Opposed to laboratory conditions, industrial fabrication procedures are usually far from perfect with respect to cleanliness and chronology of



**Table 4.** Preparation and fabrication details of the surface contamination study.

ID	Surface treatment/preparation/condition
St0	<b>Reference surface:</b> dry milled comparable to ID 3, then <i>immediately</i> EB-welded
St1	Reference surface, <b>24 h in humidor (70 % rel. Humidity)</b> , then EB-welded
St2	Reference surface, <b>48 h in humidor (70 % rel. Humidity)</b> , then EB-welded
St3	Reference surface, <b>72 h in humidor (70 % rel. Humidity)</b> , then EB-welded
St4	Reference surface, <b>14 days in humidor (70 % rel. Humidity)</b> , then EB-welded
St5	Reference surface, <b>sealing with WD40 (spray oil), 14 days in humidor (70 % rel. Humidity), cleaning with isopropanol in ultrasonic bath and drying with wipes</b> , then EB-welded
St6	Reference surface, <b>sealing with WD40 (spray oil), 14 days in humidor (70 % rel. Humidity), cleaning with soap and drying with wipes</b> , then EB-welded
St8	<b>Surface milled with coolant (industrial standard), drying with wipes</b> , then EB-welded
St9	<b>Surface milled with coolant (industrial standard), cleaning with isopropanol in ultrasonic bath and drying with wipes</b> , then EB-welded

the production steps. Both are oriented on high efficiency and easy application. Since for diffusion bonding clean surfaces are obligatory, there might be a discrepancy between optimum joining quality and commercial fabrication of large parts such as blankets.

Surface contamination includes two basically different effects, which may lead to and act as diffusion barriers, and hence, deteriorate the weld properties. Evidently, one is oxidation. This applies especially to chromium steels, where the corrosion resistance is caused by thin  $\text{Cr}_2\text{O}_3$  surface layers, which in turn suppress diffusion significantly.

The other effect literally results from dirt. In industry, this typically results from contact with oil, coolants, dust, water, wrappings, and many more. That is, prior to diffusion bonding, the surfaces have to be cleaned. And here is the problem. There might either remain traces of the cleaning agents or of the dirt or of both. In any case, such remnants could react locally with the surface during the HIP process and also act as diffusion barrier.

It is well known that 9%-Cr-steels like EUROFER rust quickly in (see-) water, in acids, or on contact with sweaty fingers. But the interesting question in connection with diffusion bonding is the rate with which an oxidation layer forms on a fresh fabricated surface in a common (industrial) environment. As has been outlined before, the perfect final surface processing step consists in dry milling. Then, before the HIP process, both surfaces have to be fixed and joined together by a circumferential and vacuum tight electron beam weld line. During industrial blanket production, there will always be a more or less extended period between both steps, and this means that more or less extended oxide layers will form.

This effect was studied by a first test series (see table 4, ID St0–St4). The reference sample ID St0 was fabricated similar to the previously described surface ID 3. It was immediately sealed vacuum tight by an EB-weld after milling. Four other samples have been put in a humidor with a constant relative humidity of 70% for 24 h, 48 h, 72 h, and for 14 days (no. 21–24) prior to sealing in the EB-weld chamber.

Finally, the samples were put in a HIP for 2 h at a pressure of 25 MPa at a temperature of 1150 °C. We increased the HIP temperature, because it is well known that diffusion bonding

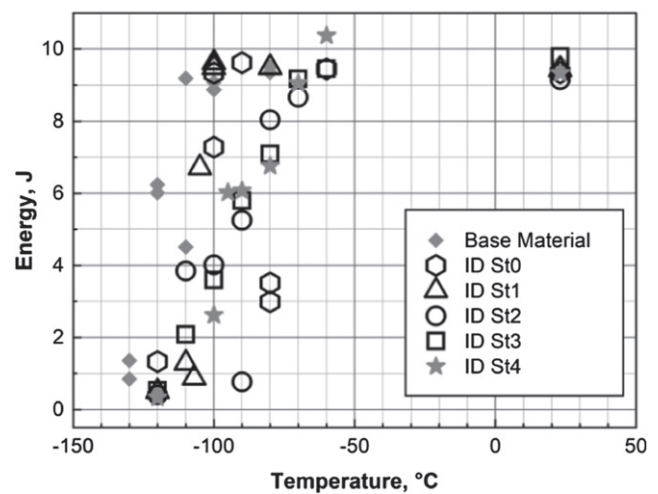


**Figure 11.** Charpy test results of the samples with different oxidation periods prior to diffusion bonding at 25 MPa, 1150 °C for 2 h and after post weld heat treatment of 980 °C/0.5 h + 760 °C/2 h. Oxidation times at 70% relative humidity: 0 h (ID St0), 1 day (ID St1), 2 days (ID St2), 3 days (ID St3), 14 days (ID St4). The scatter band indicates the base material (EUROFER97/2, heat 993 402) test results.

in the range around 1050 °C is sensitive to oxide layers. Thereafter, the standard post weld heat treatment has been applied before fabrication and testing of the Charpy specimens.

The results are plotted in figure 11. It is striking that all oxidation conditions led to the same upper shelf energies and that DBTT is shifted by only 30 K, in the worst case. Nonetheless, there is an effect from different oxidation periods: it seems that 24 h oxide formation does not deteriorate the diffusion bond considerable. After 48 h, however, there is a deterioration of DBTT, but which is not further impaired by extending oxidation periods up to 2 weeks.

Due to the appearance of significant outliers in the test results (e.g. ID St0 –80 °C), this conclusion should better be treated as a tendency and not stressed too much. On the other hand, down to test temperatures of at least –70 °C, there is no brittle fracture, independent of the oxidation period.

The effect of oxidation protection by using spray oil has been studied on two additional samples. One has been cleaned with isopropanol after 14 days oxidation in air with a relative

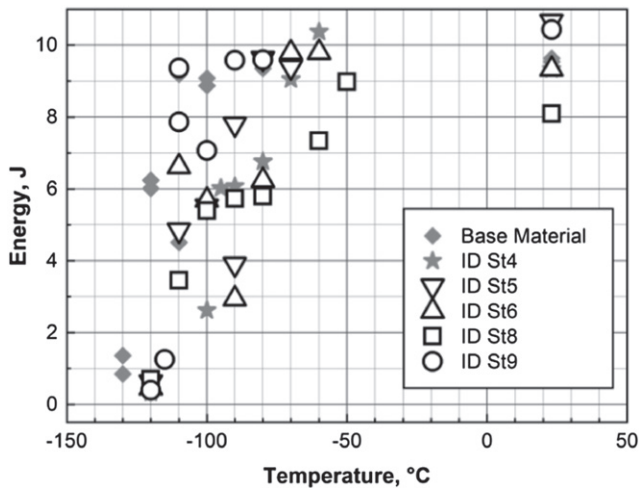


**Figure 12.** Charpy test results of samples with different cleaning and contamination treatments prior to diffusion bonding at 25 MPa, 1150 °C for 2 h and after post weld heat treatment of 980 °C/0.5 h + 760 °C/2 h. 14 days oxidation on air (ID St4), surface sprayed with oil/14 days oxidation on air/cleaning with isopropanol (ID St5), surface sprayed with oil/14 days oxidation on air/cleaning with soap (ID St6), milling with coolant/surface just wiped (ID ST8), milling with coolant/cleaning with isopropanol (ID ST9). The scatter band indicates the base material (EUROFER97/2, heat 993 402) test results.

humidity of 70%. The other has been cleaned with industry soap. The sample ID St4 from the previous study has been taken as a reference.

As can be seen from figure 12, oiling the surfaces may reduce oxidation. But obviously only isopropanol removes the oil without residues, since cleaning with soap leads to the same or even worse results compared to unprotected oxidation (scattering of the results impedes a definite assessment).

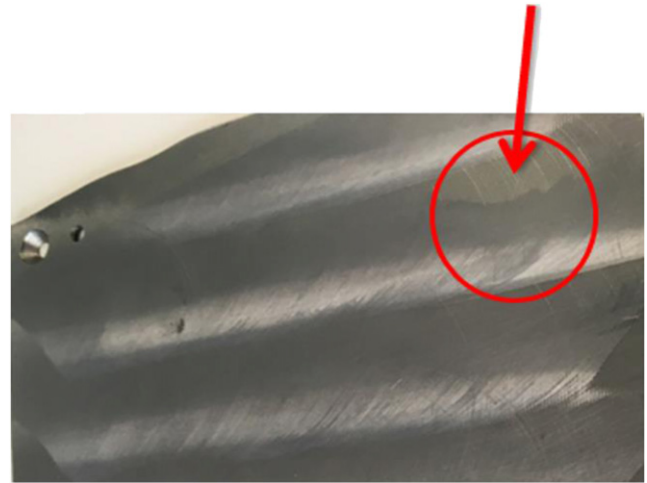
Finally, the influence of milling with coolant (as is standard in industry) on the weld quality was also studied by two samples. One sample was just wiped dry after milling (ID St8), the other was cleaned with isopropanol (ID St9).

Figure 12 shows that the use of milling coolant has no effect on the diffusion bond process, if the coolant is removed with isopropanol. Without cleaning, that is just by drying the surfaces with wipes, the weld performance is clearly deteriorated. With the exception of sample ID St8, this study leads to the same conclusion as the oxidation study: all samples (except for ID St8) show the same upper shelf energies and DBTT amounts to  $-70$  °C, even in the worst case.

Microstructure analyses of the weld interfaces confirmed optimum structural bonds in all cases: the weld surfaces were not recognizable, i.e. roughness, oxide layers, dirt and other residues did not influence the diffusion bonding.

#### 4.3. Plating

Finally, we performed the plating of a massive EUROFER97/2 block with the produced ferritic ODS steel based on the conclusions of the previous outlined studies in three steps: (1) machining the surfaces without specifications for the milling tool and parameters, (2) evacuation, degassing, and vacuum sealing in one step by a circumferential electron beam weld



**Figure 13.** ODS steel plate after removing the capsule residues and preparation of the surface for diffusion bonding. The arrow indicates one of several areas of grooves (chatter marks) that occurred due to vibrations during milling, which were used as a robustness test for the plating process.

seam, and (3) applying a high-temperature-high-pressure HIP cycle (1100 °C, 100 MPa, 2 h, Bodycote, Germany). There were also no specifications for surface cleaning and oxidation prevention.

#### 4.4. Machining the cooling channels

After joining, the combined block was milled to the final outer dimensions of 208 mm  $\times$  160 mm  $\times$  23.5 mm, reducing the thickness of the ODS steel plate to 3 mm in the process. Then the part was sent to KRÜGER ERODIERTECHNIK for electro-discharge wire-cutting the cooling channels according to the drawing in figure 4 (more details are given in [24–26]). This commercial fabrication step can also be performed on real-size components up to 3 m length.

### 5. Mockup testing

#### 5.1. Process robustness tests

Milling down the ODS steel plate's surfaces to remove the leftovers of the stainless-steel capsule, proved to be challenging due to residual stresses left in the material after cross rolling. Even tempering at 800 °C for 2 h did not completely remove these stresses. Therefore, we fixed the plate by holes in the border area onto a holder during milling. Nevertheless, chatter marks (grooves) formed due to vibrations, which led to an unusual rough surface (see figure 13). Since such imperfections might have to be tolerated in an industrial production, we continued the mock-up fabrication and took this as an occasion for a robustness test.

An additional general test for the robustness of the mock-up design and also for possible off-normal process conditions or for deviations from process specifications was introduced by the intentional misalignment of the middle cooling channel. Here, the weld seam of the ODS steel plating was placed along both upper corners of the channel, which are the highest

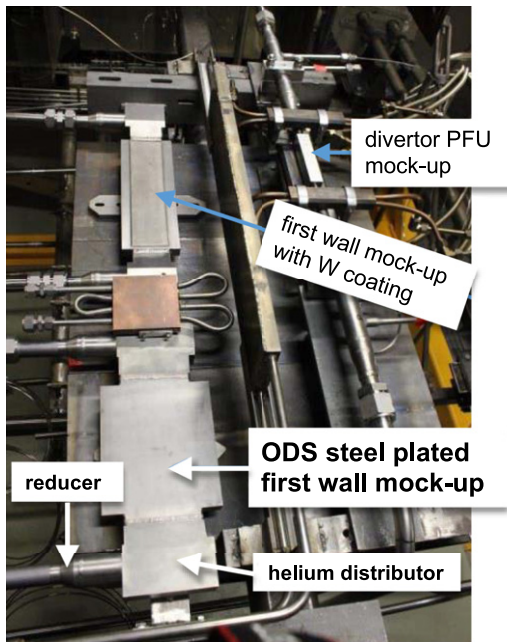


**Figure 14.** Testing chamber of the HELOKA facility. Beside our ODS steel plated first wall mock-up, there was another first wall and a divertor mock-up installed on the same test frame.

stressed locations, and therefore, act as crack initiation lines. Our intention was to speed up damage or failure of the mock-up during the high-heat flux tests, since the available facility time was limited and sufficed only for a few hundred cycles.

### 5.2. Test environment and instrumentation

Within the EUROfusion breeding blanket work package, sub-component tests in helium facilities were scheduled. We took this as an opportunity to modify and extend an already planned campaign to test our first wall mock-up in the HELOKA. We designed the experimental setup for a parallel installation of two mock-ups next to each other in the HELOKA vacuum tank, that is, one test position for our mock-up and another for a FW mock-up with functional-grading W/EUROFER coating. Due to the similarity of the channel geometry of the two mock-ups, a common design for the helium distributor, which connects one inlet and outlet pipe to the cooling channels, was developed. The installation in the testing chamber is shown in figure 14.

The helium distributors have been designed considering a total mass flow rate of  $40 \text{ g s}^{-1}$  in each channel (i.e.  $200 \text{ g s}^{-1}$  in total), an inlet temperature of  $300 \text{ }^\circ\text{C}$  and an inlet pressure of  $8 \text{ MPa}$ . The mass flow distributions of the different designs have been evaluated based on CFD analyses. The final mock-up consists of five parts: the mock-up plate with five cooling channels, two helium distributors, and two reducers. Before these parts can be joined, the first wall plate had to be modified by milling connectors on both ends that fit to the distributors. All parts were tungsten-inert-gas (TIG) welded, followed by a post-welding heat treatment (PWHT). Finally, the welds were examined by liquid penetration as well as by ultra-sonic testing. More details can be found in [27]. Both

**Table 5.** High heat flux fatigue test sequences for the mock-up in the helium loop at KIT (HELOKA facility).

Test sequence	Cycles	Heat flux ( $\text{MW m}^{-2}$ )	Pulse length (on/off)	Surface temperature
#1	100	0.7	2 min/2 min	$\sim 550 \text{ }^\circ\text{C}$
#2	100	0.8	2 min/2 min	$\sim 600 \text{ }^\circ\text{C}$
#3	100	0.9	2 min/2 min	$\sim 650 \text{ }^\circ\text{C}$
#4	7	0.9	2 h/>2 min	$\sim 650 \text{ }^\circ\text{C}$

revealed no cracks or leaks. The facility and mock-up were instrumented to measure and record the following parameters during the experiment for relevant points in time: mock-up surface temperature by infra-red (IR) camera, helium inlet/outlet temperatures, the total mass flow, and the absolute helium inlet pressure. Before the installation of the mock-up in HELOKA, a pressure test according to EN 13455–5:2014 with helium gas was completed.

### 5.3. High heat flux tests

The European DEMO operating scenario for the starter blankets includes cycle numbers in the order of 10 000. Since that would have exceeded our available testing time contingent, the emphasis of this first experiment was rather placed on probing higher surface temperatures (i.e.  $600 \text{ }^\circ\text{C}$  or even higher) than on reaching realistic cycle numbers. The test matrix has been defined based on finite element simulations and thermo-mechanical analyses of various loading configurations and coolant inlet temperatures that would guarantee the structural integrity of the mock-up during the test cycles at high surface temperatures. The stresses in the mock-up have been evaluated according to the RCC-MRx code.

After initial tests, the mock-up was loaded according to the defined goals, that is, high heat flux tests were carried out by operating the test facility in the reference scenario. Here the electron beam was switched on and off in 2 min intervals for a predefined number of cycles. Three fatigue test sequences with 100 cycles each were conducted, resulting in surface temperatures of  $550 \text{ }^\circ\text{C}$ ,  $600 \text{ }^\circ\text{C}$ , and  $650 \text{ }^\circ\text{C}$ . Then a final sequence of 7 cycles with a pulse length of 2 h was performed (see table 5).

During the first three sequences, the operating parameters remained within safe margins, indicating that the mock-up did not start to crack or fail. The remaining operating time for testing our mock-up was then used for a longer-pulse exposure at  $650 \text{ }^\circ\text{C}$  surface temperatures. During the 7 pulses of 2 h each, creep or other thermal effects might have been activated that would damage the mock-up in the one or other way. However, a peculiar change in the operating parameters did not appear, which indicated that the structural integrity was (most probably) not affected.

In summary, the performed four test sequences of more than 300 high heat flux cycles in total can be marked as a full success. The predefined goals have not only been reached, but were even exceeded.



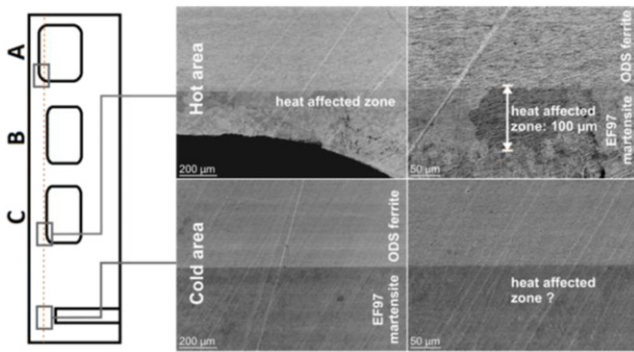


**Figure 15.** (Left) Technical drawing and identification of the cooling channel cross-sections A, C (hot area), and cold area. (Right) Comparison of the BSE images acquired in the ODS steel/EUROFER97 (EF97) interfacial area in the hot area close to channel C and in a cold outer region at different magnifications. A heat affected zone can be recognized clearly in the hot interface area. In the BSE image of the cold area reveals only a hint (therefore the question mark) of a heat affected zone.

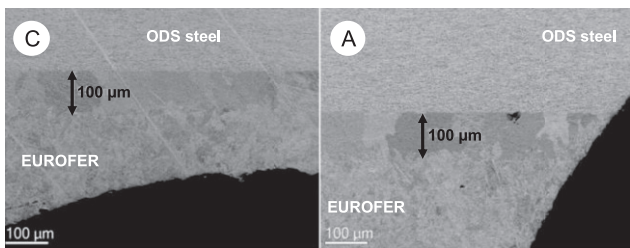


**Figure 16.** Comparison of the BSE images acquired in the ODS/EF97 interfacial region close to channel C (left) and channel A (right). The imaging areas are indicated in figure 15. Both images reveal a distinct formation of a heat affected zone between ODS and EUROFER steel with a thickness of about 100  $\mu\text{m}$ .

## 6. Post test examinations

After the high heat flux testing, we wanted to identify and investigate possible microstructural changes, defects, and surface modifications in the assumed critical zones of the mock-up. For this, several cross-sections through the mock-up were cut and prepared for optical and electron microscopy, i.e. scanning electron microscopy and back scattering electron (BSE) imaging. Prior to the microstructure analysis, a representative piece of the mock-up was selected and the mock-up was cut apart accordingly, which is illustrated in figure 15.

BSE images of the ODS steel/EUROFER97 weld interface were acquired close to the corners of channels A and C, which are the high heat flux loaded hot areas (figure 16). For comparison, an image from a cold region is also shown in figure 15. On the EUROFER side of the interface, an area of about 100  $\mu\text{m}$  in width is recognizable that contains larger grains. In the following, we denote this area as heat affected zone (HAZ). However, the HAZ is clearly recognizable in the hot area, only.

Besides the structural changes that can be observed by imaging, chemical changes in the vicinity of the weld interface are also of interest. For this, we acquired SEM-EDX elemental maps (note: they are not illustrated here) in and outside

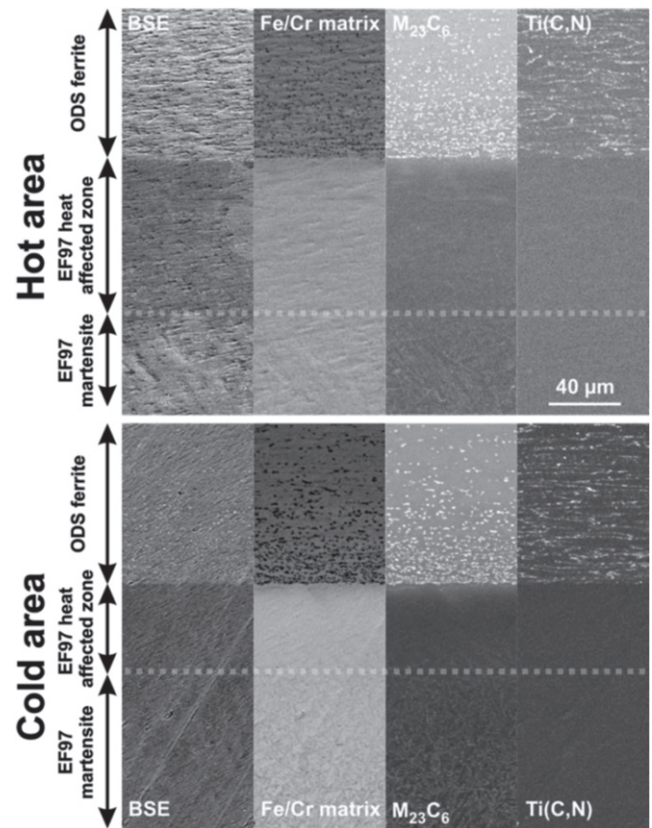


**Figure 17.** PCA of SEM-EDX data. It reveals the single phases, which are present in the respective sample areas. The heat affected zones are indicated by dotted lines.

of the HHF loaded area, in which the W and the Cr maps show martensitic needle structure only in the lower part of the EUROFER97 region in both areas. Therefore, the open question regarding the discussion of the cold area in figure 15 is answered: there is a HAZ in the cold area, too, and therefore, it developed already in the diffusion bonding process.

Moreover, we could successfully determine the involved phases by performing a principal component analysis (PCA) on both SEM-EDX datasets. In both areas, three phases (factors) were found: Fe/Cr matrix, Cr/W carbides (i.e.  $\text{M}_{23}\text{C}_6$ ), and Ti carbo-nitrides. The PCA map is plotted in figure 17. EDX and PCA enabled us further to determine the width of the HAZs, which was not possible by analysing the BSE image in the cold area. The width of the HAZ in the cold area (based on a measurement of the region without recognizable martensite laths or needles) amounts to about 55–60  $\mu\text{m}$ , which is less than the 90–100  $\mu\text{m}$  found in the HHF zone.

Thus, we conclude that the formation mechanism of the HAZ has two stages: the first one is due to diffusion bonding and the second one is due to HHF testing. Both processes provide conditions in which Cr and C diffusion can take place: during diffusion bonding the temperature is 1100  $^{\circ}\text{C}$  for 2 h and during the HHF test sequences 3 and 4 the interface is heated up to more than 500  $^{\circ}\text{C}$  for more than 15 h (according to a simulation of the area between the channels—in the interface directly over the channels, the temperature is even higher).

The width of the Cr diffusion zone (from the ODS ferrite into the EUROFER martensite) is comparable in both, the hot and the cold area. The density of Cr-rich precipitates in the ODS ferrite (white dots in the  $M_{23}C_6$  maps in figure 17) is increasing towards the interface. The Ti–K map shows Ti-rich precipitates in the ODS ferrite (white dots in the Ti(C,N) maps in figure 17), likely at grain boundaries. The overall precipitation structure in the ODS ferrite is similar in both areas.

As outlined in section 5.1, we implemented two features in the mock-up as a robustness test: (1) crack initiators in the upper corners of cooling channel A, and (2) chatter marks in the surface of the ODS steel plate. After thorough inspection of all cross-sections, sample parts, and specimens there was no indication of defects, like, pores, cracks, delamination, Kirkendall voids, or other faults.

## 7. Conclusions

For future fusion power plants, but also for the blanket concepts of DEMO reactors, operating temperatures in the range of 450–550 °C (or possibly higher) could be an effective measure to reduce irradiation hardening of the structural materials, like martensitic 8–9Cr steels (EUROFER97, F82H, and others) significantly. In this case, the lifetime of breeding blankets (in particular helium-cooled components) would then mainly be determined by the thermo-mechanical load response (thermal fatigue) and by the accumulation and growth of helium bubbles due to unavoidable transmutation. The presented strategy could possibly overcome or at least mitigate the related design limits. It consists of plating the plasma-facing surface of the blankets with thin ODS steel plates. Nevertheless, a more effective strategy, but harder to realize, would be the replacement of EUROFER by ODS steel within a layer of about 300 µm, or even completely.

Referring to the outline of the current project as presented in the introduction section, we want to highlight the following assessments and outcomes: (1) we demonstrated the availability, maturity, and robustness of industrial fabrication, machining, and production processes, which are required for ODS steel plating of flat blanket first walls. (2) By such plating, the surface operating temperature of a helium-cooled first wall mock-up could be increased to 650 °C for 100 heat flux pulses of 2 min and for additional 7 cycles of 2 h each. (3) The mock-up removed a heat flux of 0.9 MW m<sup>-2</sup> by helium cooling without swirls, flow enhancers or other measures for an increased heat transfer. (4) The mock-up did not develop cracks or other tendencies to fail. Even at intentionally introduced weak points (crack initiators), crack formation did not occur. (5) Post-experimental microstructural analyses by SEM did not reveal weld or production voids. Also, critical changes like Kirkendall pores did not develop in and outside the interface region. (6) The following microstructural features were recognized and analysed: (i) a coarse grained heat affected zone formed in the EUROFER part below the interface. This is most probably due to the carbon concentration gradient (0.1% C in EUROFER, C is just a contamination in the ODS steel)

that leads to C diffusion into the ODS steel. In the EUROFER region, the C depletion leads then to a transformation from martensite to ferrite. (ii) Two fractions of precipitates were found inside the ODS plate: (a) Cr carbides and (b) Ti(C,N). (iii) The Cr precipitate density increases in the ODS steel towards the interface due to C diffusion from the EUROFER steel. (iv) The Cr diffusion into the EUROFER zone is 5 times smaller compared to the heat affected zone.

For an improved blanket concept, the formation of the recognized heat affected zone should be prohibited, because the ferrite could tend to embrittlement under neutron irradiation, which could lead to crack formation. The easiest solution consists in the use of an ODS and EUROFER steel type with the same carbon content. This is the case, for example, for EUROFER97 and the 9Cr ODS–EUROFER steel. Of course, a full replacement of EUROFER steel by an ODS steel would also settle the matter.

## Acknowledgments

We want to thank Daniel Bolich and Rainer Ziegler, both from Karlsruhe Institute of Technology (KIT, IAM), for their support regarding organization and dealing with infrastructural tasks like coordination of machining, photographing, and sample preparation. We are also grateful to the KIT CN workshop team with a special thanks to Tanja for the excellent EDM performance. Many thanks go to the group of chemical analysis headed by Thomas Bergfeld, KIT, IAM. Generally, we wish to express our gratitude to all colleagues who were involved the one or other way in this project. This work has been carried out within the framework of the EUROfusion Consortium and has received funding from the Euratom research and training program 2014–2018 and 2019–2020 under Grant Agreement No. 633053. The views and opinions expressed herein do not necessarily reflect those of the European Commission.

## ORCID iDs

M. Rieth  <https://orcid.org/0000-0002-6231-6241>  
 G. Pintsuk  <https://orcid.org/0000-0001-5552-5427>  
 B.-E. Ghidersa  <https://orcid.org/0000-0002-7863-6290>  
 E. Simondon  <https://orcid.org/0000-0002-8094-281X>

## References

- [1] Federici G., Biel W., Gilbert M.R., Kemp R., Taylor N. and Wenninger R. 2017 European DEMO design strategy and consequences for materials *Nucl. Fusion* **57** 092002
- [2] Federici G. et al 2018 *Fusion Eng. Des.* **136** 729–41
- [3] Federici G., Boccaccini L., Cismonti F., Gasparotto M., Poitevin Y. and Ricapito I. 2019 An overview of the EU breeding blanket design strategy as an integral part of the DEMO design effort *Fusion Eng. Des.* **141** 30–42
- [4] Federici G. et al 2019 Overview of the DEMO staged design approach in Europe *Nucl. Fusion* **59** 066012

- [5] Klimenkov M., Möslang A. and Materna-Morris E. 2014 Helium influence on the microstructure and swelling of 9%Cr ferritic steel after neutron irradiation to 16.3 dpa *J. Nucl. Mater.* **453** 54–9
- [6] Materna-Morris E., Lindau R. and Moslang A. 2010 Modifications of alloying elements in martensitic 8%–10% Cr-steels and its influence of neutron irradiation on material properties *Mater. Sci. Forum* **636–637** 631–6
- [7] Klimenkov M., Möslang A., Materna-Morris E. and Schneider H.-C. 2013 Helium bubble morphology of boron alloyed EUROFER97 after neutron irradiation *J. Nucl. Mater.* **442** S52–7
- [8] Klimenkov M., Jäntsch U., Rieth M. and Möslang A. 2020 Correlation of microstructural and mechanical properties of neutron irradiated EUROFER97 steel *J. Nucl. Mater.* **538** 152231
- [9] Brabänder A.V., Bredl J., Schneider H.-C. and Kamlah M. 2019 Registering hardness measurement of neutron-irradiated low-activation steels at high temperatures *Fusion Eng. Des.* **146** 2734–7
- [10] Dethloff C., Gaganidze E. and Aktaa J. 2018 Review and critical assessment of dislocation loop analyses on EUROFER 97 *Nucl. Mater. Energy* **15** 23–6
- [11] Schneider H.-C., Petersen C., Povstyanko A.V., Fedoseev A.E. and Makarov O. 2017 Repeatability of irradiation damage and of recovery by post-irradiation annealing of EUROFER base steels *Fusion Eng. Des.* **124** 1019–23
- [12] Klimenkov M., Lindau R., Jäntsch U. and Möslang A. 2017 Effect of irradiation temperature on microstructure of ferritic-martensitic ODS steel *J. Nucl. Mater.* **493** 426–35
- [13] Materna-Morris E., Schneider H.-C. and Möslang A. 2014 Tensile behavior of RAFM alloys after neutron irradiation of up to 16.3 dpa between 250 and 450 °C *J. Nucl. Mater.* **455** 728–34
- [14] Gilbert M.R., Dudarev S.L., Zheng S., Packer L.W. and Sublet J.-C. 2012 An integrated model for materials in a fusion power plant: transmutation, gas production, and helium embrittlement under neutron irradiation *Nucl. Fusion* **52** 083019
- [15] Sato S. and Maki K. 2003 Analytical representation for neutron streaming through slits in fusion reactor blanket by Monte Carlo calculation *Fusion Eng. Des.* **65** 501–24
- [16] Zinkle S.J. and Snead L.L. 2014 Designing radiation resistance in materials for fusion energy *Annu. Rev. Mater. Res.* **44** 241–67
- [17] He P., Klimenkov M., Möslang A., Lindau R. and Seifert H.J. 2014 Correlation of microstructure and low cycle fatigue properties for 13.5Cr1.1W0.3Ti ODS steel *J. Nucl. Mater.* **455** 167–73
- [18] Straßberger L., Chauhan A., Czink S. and Aktaa J. 2017 High-temperature low-cycle fatigue behavior and microstructural evolution of an ODS steel based on conventional T91 *Int. J. Fatigue* **100** 50–7
- [19] Chauhan A., Hoffmann J., Litvinov D. and Aktaa J. 2018 High-temperature low-cycle fatigue behavior of a 9Cr-ODS steel: Part 2. Hold time influence, microstructural evolution and damage characteristics *Mater. Sci. Eng. A* **730** 197–206
- [20] Hoelzer D.T., Unocic K.A., Sokolov M.A. and Byun T.S. 2016 Influence of processing on the microstructure and mechanical properties of 14YWT *J. Nucl. Mater.* **471** 251–65
- [21] Zinkle S.J., Boutard J.L., Hoelzer D.T., Kimura A., Lindau R., Odette G.R., Rieth M., Tan L. and Tanigawa H. 2017 Development of next generation tempered and ODS reduced activation ferritic/martensitic steels for fusion energy applications *Nucl. Fusion* **57** 092005
- [22] Ukai S. and Fujiwara M. 2002 Perspective of ODS alloys application in nuclear environments *J. Nucl. Mater.* **307–311** 749–57
- [23] Raj B. and Vijayalakshmi M. 2012 Ferritic steels and advanced ferritic-martensitic steels *Compreh. Nucl. Mater.* **4** 97–121
- [24] Hernández F.A. et al 2018 Overview of the HCPB research activities in EURO fusion *IEEE Trans. Plasma Sci.* **46** 2247–61
- [25] Hernández F.A. et al 2019 An enhanced, near-term HCPB design as driver blanket for the EU DEMO *Fusion Eng. Des.* **146** 1186–91
- [26] Hernández F.A. et al 2019 Advancements in the helium-cooled pebble bed breeding blanket for the EU DEMO: holistic design approach and lessons learned *Fusion Sci. Technol.* **75** 352–64
- [27] Rieth M. et al 2021 Impact of materials technology on the breeding blanket design—recent progress and case studies in materials technology *Fusion Eng. Des.* **166** 112275